Open Access

Catalysis Research

LIDSEN Publishing Inc.

Original Research

Determination of Reflectance Spectra and Colorimetry of Titanium and Tungsten Oxides Obtained by Microwave-assisted Hydrothermal Synthesis

Luana Góes Soares [1, 2, †, *], Sandra Kunst [1, †], Cláudia Trindade Oliveira [1, †], Annelise Kopp Alves [2]

1. Feevale University, Laboratory for Advanced Studies in Materials, Campus II, RS 239, 2755, Novo Hamburgo, Brasil; E-Mails: lugoes.soares@gmail.com; tessaro@gmail.com; cto@feevale.br
2. Federal University of Rio Grande do Sul, Ceramic Materials Laboratory, Avenida Osvaldo Aranha, 99 room 709, Porto Alegre, Brasil; E-Mail: annelise.alves@ufrgs.br

† These authors contributed equally to this work.

* **Correspondence:** Luana Soares; E-Mail: lugoes.soares@gmail.com

Academic Editor: Giane Gonçalves Lenzi

Special Issue: Advance in Photocatalysis

Catalysis Research
2024, volume 4, issue 3
doi:10.21926/cr.2403007

Received: February 04, 2024
Accepted: June 20, 2024
Published: July 01, 2024

Abstract

Sustainability has driven the use of heterogeneous photocatalysis as one of the primary methods for environmental decontamination, reduction, degradation, remediation, or transformation of polluting chemical residues and purification treatment of effluents and wastewater. TiO_2 is the most commonly used semiconductor in heterogeneous photocatalysis. It acquires relevance, as it has favorable properties, such as non-toxicity, stability in a wide range of pH, economic viability, etc., which encourage its application as a semiconductor in photocatalytic processes. However, the photocatalytic capabilities of TiO_2 are only active in 3% of the solar spectrum, which limits its range of use. For this reason, some semiconductor metal oxides were incorporated into TiO_2 to increase its activation range in the UV-visible spectrum. Within this context, WO_3 is a metallic oxide widely used in mixtures with TiO_2, aiming to improve its photocatalytic properties. Thus, this work synthesized TiO_2 and TiO_2

nanostructures mixed with two tungsten precursors (H_2WO_4 and $Na_2WO_4.2H_2O$) using a microwave-assisted hydrothermal route at 200°C for 120 minutes. The samples obtained were characterized by mL of a 20 ppm solution of methyl orange dye. The results show that it was possible to successfully produce TiO_2 and TiO_2 nanostructures containing tungsten precursors via a microwave-assisted hydrothermal route. This can be attributed to the fact that the energy associated with this temperature was sufficient to convert most of the precursors into crystalline products and little amorphous phase is present.

Keywords
Hydrotermal; microwave-assisted; photocatalysis; TiO_2; tungsten

1. Introduction

Environmental issues associated with the high cost necessary for the implementation of new treatment processes aiming at sustainability have boosted the use of heterogeneous photocatalysis as one of the main methods used in environmental decontamination, reduction, degradation, remediation or transformation of polluting chemical residues, treatment effluents and wastewater purification [1].

In this context, the use of photocatalysts in degrading dyes has been growing. These materials have proven to be effective in remediation due to their non-toxicity and because they are economically viable [2].

TiO_2 is the most commonly used semiconductor in heterogeneous photocatalysis. It acquires relevance due to its efficiency in the decomposition of pollutants in water, air, bacteria, and cancer cells and in the degradation of toxic organic compounds, in addition to having favorable properties, such as non-toxicity, stability over a wide pH range, being viable economically, etc., which stimulate its application as a semiconductor in photocatalytic processes. However, the photocatalytic capabilities of TiO_2 are only active in 3% of the solar spectrum, which limits its range of use. For this reason, some semiconductor metal oxides have been incorporated into TiO_2 in order to increase its activation range in the UV-visible spectrum [1-3].

Several methods have been used in the synthesis of photocatalysts. Some examples include electrospinning, sol-gel, impregnation, microemulsion, hydrothermal and mechanical methods [1, 3].

Within this context, WO_3 is a metallic oxide widely used in mixtures with TiO_2, aiming to improve its photocatalytic properties. According to the literature, the coupling of WO_3 to TiO_2 improves the photodegradation capacity of TiO_2, as it inhibits the recombination of the electron/hole pair, increasing the light absorption range and activation of visible spectra. It also functions as an electron trap, which leads to obtaining photochromic materials with energy storage capacity due to the formation of agglomerates on the surface of samples containing tungsten, which function as electron traps [1, 3].

Tungsten trioxide (WO_3) gained prominence due to its applications in electrochromic, photochromic, photocatalytic materials and gas sensors, such as information storage media, data display, optical signal processing, intelligent windows, and the like. They have also been applied as

nanostructured semiconductors, aiming to improve semiconductor materials' properties and future applications, such as TiO_2 [4].

WO_3 is a metallic oxide with an n-type configuration. Its crystalline structure is similar to rhenium trioxide (ReO_3), an ABO_3-type perovskite structure without cations. It has several crystalline structures, which appear depending on the heat treatment temperature: tetragonal, monoclinic, orthorhombic, and triclinic. The monoclinic phase is almost always considered the most stable crystalline phase structure of WO_3 [4].

Although the hydrothermal method is widely used to synthesize different types of materials, such as nanometric oxides to from binary oxides (e.g., ZnO, CuO, MgO, TiO_2, SnO_2) and ternary oxides ($BaTiO_3$, $PbTiO_3$, $BiFeO_3$, $KNbO_3$), and others of complex stoichiometry ($Ba_{1-x}Sr_xTiO_3$, $La_{0.5}Ca_{0.5}MnO_3$, $La_{0.325}Pr_{0.300}Ca_{0.375}MnO_3$), the reaction kinetics is slow. A factor that drives the application of the method hydrothermal heat in conjunction with microwave heating. The joint action of these two methods raises the heat treatment temperature more rapidly, increasing the reaction kinetics [5].

Among the main advantages of this method is the possibility of proceeding with the synthesis at lower temperatures, compared to solid-state and vapor-phase reactions, for example. It also enables the formation of crystalline products without the need for subsequent heat treatment, a high heating rate, a significant reduction in synthesis time, and a low synthesis temperature.

Obtaining nanostructures through hydrothermal synthesis involves a solution in which pressure and temperature change, altering the chemical responses. Therefore, the current equipment reactions take about a day to be carried out and take place in processes that can be applied to organic and inorganic materials [1, 3].

The present work proposes the synthesis of TiO_2 added to 2 different tungsten precursors ($Na_2WO_4.2H_2O$ and H_2WO_4) by microwave-assisted hydrothermal route. We aim to increase the degradation capacity through the decolorization of 125 mL of a 20 ppm solution of methyl orange dye and increase the light absorption range of TiO_2 in the visible region. As far as we know, such a study on the correlation of optical and photocatalytic properties using the tungsten precursors mentioned above has been minor or never reported.

2. Materials and Methods

2.1 Experimental

As reagents, P25 (Evonik, 99.5% purity, Sigma Aldrich), titanium tetraisisopropoxide (TIP, 99.99% purity, Sigma Aldrich), polyvinylpyrrolidone (PVP, 99.99% purity, Sigma Aldrich), glacial acetic acid (purity 99.8%, Sigma Aldrich), hydrogen peroxide (35% purity, aqueous solution, Dynamic), sodium tungstate dihydrate ($Na_2WO_4.2H_2O$, 99.0% purity, Dynamic), tungstic acid (H_2WO_4, 98.0% purity, Sigma Aldrich), orange of methyl (analytical grade, 85% purity, Sigma Aldrich) and ethyl alcohol (99.5% purity, Dynamics), reagents were used without further purification.

2.1.1 Obtaining Samples of Titanium and Tungsten Oxides

TiO_2, TiO_2/WO_3 and $TiO_2/Na_2WO_4.2H_2O$ nanostructures were synthesized following an adaptation of the route described in the work of Chang et al., 2009 [5]. In the present work, the titanium tetraisopropoxide reagent was used as a precursor and source of titanium. Initially, 3 solutions were prepared:

i. TiO_2- 2.5 mL of titanium tetraisopropoxide added to 15 mL of isopropyl alcohol, 2.0 mL of glacial acetic acid, 5 mL of polyvinipyrrolidone (PVP). The mixture was homogenized by magnetic stirring for approximately 5 minutes.
ii. WO_3- In a 250 mL beaker, 1.0 g of tungstic acid (H_2WO_4), 5.0 mL of PVP and 100 mL of H_2O_2 were added. Where the mixture remained under magnetic stirring for 2 hours.
iii. TiO_2/WO_3- 2.5 mL of titanium tetraisopropoxide added to 15 mL of isopropyl alcohol, 2.0 mL of glacial acetic acid, 5 mL of polyvinipyrrolidone (PVP) and 0.10 g of tungstic acid (H_2WO_4). This mixture was homogenized by magnetic stirring for approximately 5 minutes, and then 1 mL of hydrogen peroxide (H_2O_2) was slowly added to the mixture.
iv. $TiO_2/Na_2WO_4.2H_2O$- 2.5 mL of titanium tetraisopropoxide added to 15 mL of isopropyl alcohol, 2.0 mL of glacial acetic acid, 5 mL of polyvinipyrrolidone (PVP) and 0.10 g of sodium tungstate dihydrate ($Na_2WO_4.2H_2O$). This mixture was homogenized by magnetic stirring for approximately 5 minutes, and then 1 mL of hydrogen peroxide (H_2O_2) was slowly added to the mixture.

The resulting solutions, one at a time, were placed in a Teflon-coated flask and subjected to a microwave oven (MDS-8G, manufactured by Shanghai Sineo Microwave Chemistry Technology Co., Ltd). The heat treatment was conducted at different times (30, 60 and 120 min) and temperatures (100, 150 and 200°C). The synthesis reactions were performed in triplicates.

2.1.2 Characterization of the Powders Obtained

The crystalline phases in the samples obtained were identified by a Philips diffractometer, model X'pert MPD, with CuKα radiation (λ = 0.1541 nm), which operates at 40 kV and 40 mA, with a step of 0.025°/2 s in a range of 2θ to 80°. The diffraction patterns obtained were compared to the JCPDS database (Joint Committee on Powder Diffraction Standards) using the X'Pert HightScore® software. The morphology of the samples was investigated using an EVO MA10 - Carl Zeiss scanning electron microscope, which operates at 20 kV. The surface area and porosity were evaluated using the Brunauer Emmett and Teller (BET) method and the Autosorb Quantachrome, Nova 1000e instruments. Colorimetry analyses were performed using a spectrophotometer (Konica-Minolta, CM 2600 d) with a sphere integrated into an ultra-violet filter. The spectrophotometer uses the D65 illuminant, corresponding to the daylight's spectral range. The measurement of the color reflected by the sample simulates an observer at 10°. The instrument is calibrated before the analysis, using two points as a reference, zero and standard blank. The spectrophotometer works in conjunction with i7 software that comes with the equipment. To carry out the photocatalysis tests, 50 mg of TiO_2, TiO_2/WO_3, $TiO_2/Na_2WO_4.2H_2O$, and P25 standard powders were mixed, one at a time, with 125 mL of a 20 ppm dye solution methyl orange. The mixtures, one at a time, were transferred to an ultrasound (Cole-Parmer CP-750) and kept in a dark place for 15 minutes to: dissociate possible particle agglomerates from the mixing, better dispersion of the material and, initial adsorption of the dye on the surface of the catalyst. After the end of the homogenization period, the solutions, one at a time, were transferred to a photocatalytic reactor with the UV light system on. Before the start of each assay, a 4 mL aliquot of the solution was collected, defined as the initial reference sample (absorbance indicative of the initial concentration of methyl orange; reaction time of zero minutes).

This first aliquot was removed before applying the light system, water circulation, and air bubbling. After starting the assay, 4 mL aliquots were withdrawn with a syringe at 15-minute intervals, filtered through a 0.2 µm filter, and transferred to polymethylmethacrylate (PMMA) cuvettes. Then, the aliquots were analyzed for their absorbance (Cary 5000, Agilent, with UMA accessory). Diffuse reflectance measurements were performed using an Agilent spectrophotometer, model Cary 5000, equipped with an integrating sphere model DRA-1800. Band gap energies were calculated using the Kubelka-Munk [6] function (Equation 1).

$$\frac{K}{S} = \frac{(1-R)2}{2R} \quad (1)$$

Where:
K is the absorption coefficient;
S is the dispersion coefficient and
R is the spectral reflectance fator.

3. Results

3.1 X-Ray Diffraction (XRD)

The diffraction patterns of TiO_2 samples synthesized at 100°C are shown in the Figure 1. According to the results, a baseline with a lot of noise can be verified in each diffractogram, mainly in the samples submitted to the hydrothermal treatment for 30 minutes, possibly indicating the presence of amorphous phases [7]. The anatase phase (PDF 00-001-0562) was most clearly identified in the XRD patterns of samples subjected to hydrothermal treatment for 120 minutes.

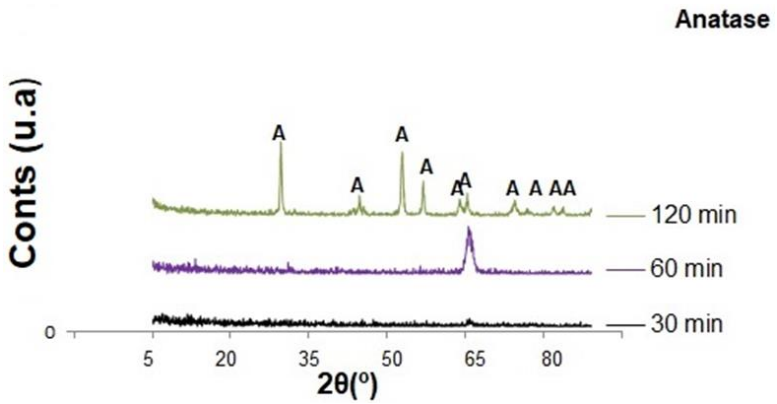

Figure 1 Caption 3. Diffractogram of TiO_2 samples synthesized at 100°C for 30, 60 and 120 minutes.

Our result is in agreement with Costa et al. [8]. They also observed in his work only the formation of the single crystalline phase of anatase, with corresponding diffraction peaks identified by diffraction spectrum. This showed only O-Ti-O ligations corresponding to the TiO_2 phase and a considerable enlargement, thus indicating the nanometric characteristics of TiO_2 powder particles.

The diffractogram of the TiO_2 sample prepared by hydrothermal synthesis at 150°C and 200°C shows peaks of the anatase phase (PDF 00-001-0562), respectively. Note that for the samples prepared at 150°C and 200°C, the amorphous phase decreased considerably compared to the

sample prepared at 100°C in Figure 2. Thus, it was assumed that the crystallinity of the samples increased as a consequence of the increase in the synthesis temperature. The crystallinity of the TiO_2 samples synthesized in this work is more excellent than, for example, the crystallinity observed in the work by Sun et al., 2019 [5], where TiO_2 obtained a low crystallinity. They noticed that the peak intensities in the XRD patterns of the samples gradually increased with the increase in calcination time or temperature, which agrees with the results obtained in the present work.

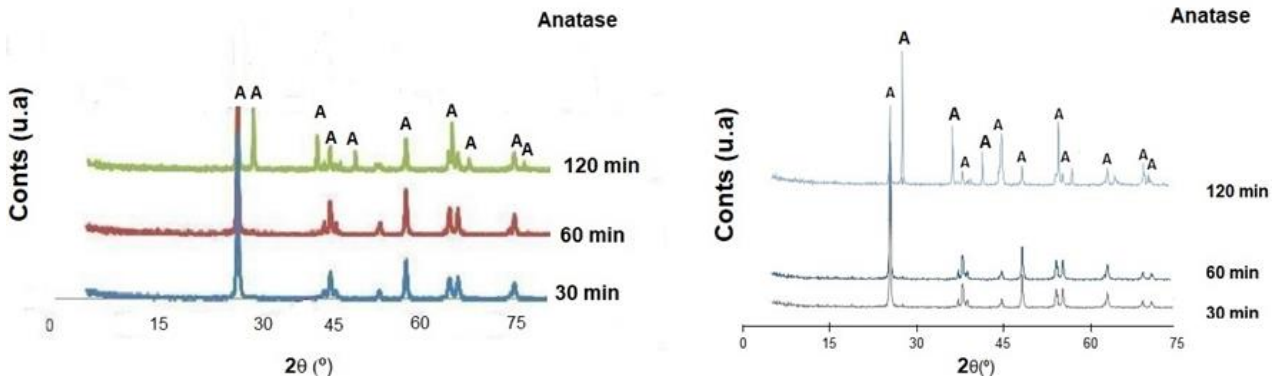

Figure 2 Caption 3. Diffractogram of TiO_2 samples synthesized at 150°C and 200°C for 30 min, 60 min and 120 min.

The diffraction patterns of TiO_2/WO_3 samples sintered at 100°C are shown in Figure 3. According to the results, one can identify the formation of the anatase phase (PDF 00-001-0562) for TiO_2 and the presence of the orthorhombic phase for WO_3.

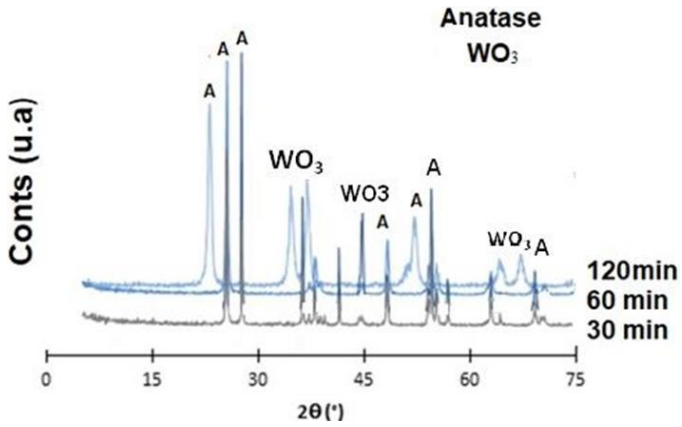

Figure 3 Caption 3. Diffractogram of TiO_2/WO_3 samples sintered at 100°C.

The diffraction patterns of the TiO_2/WO_3 samples sintered at 150°C are shown in Figure 4. According to the results, one can identify the formation of the anatase phase (PDF 00-001-0562) and rutile for TiO_2, as well as the presence of the orthorhombic phase for WO_3 (PDF-).

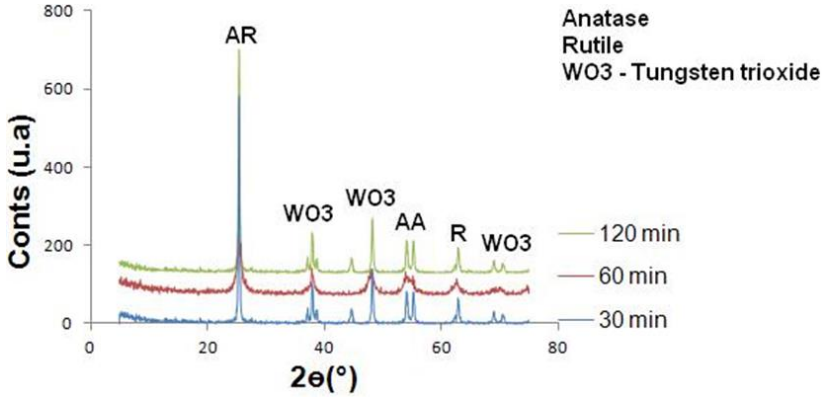

Figure 4 Caption 3. Diffractogram of TiO_2/WO_3 sample sintered at 150°C.

In both diffraction patterns of TiO_2/WO_3 samples sintered at 100°C and 150°C, respectively, one can identify the formation of the anatase (PDF 00-001-0562) and rutile phase for TiO_2, and also the presence of orthorhombic phase for WO_3 (PDF-541012). The sharp peak at approximately θ = 30° suggests that rutile is highly crystalline. It is also noticed that regardless of the sintering temperature, the same orthorhombic WO_3 phase (PDF 54-1012) is formed. This was also observed by Pan *et al*. [9] when performing the hydrothermal synthesis of their samples.

A decrease in the intensity of the diffraction peaks is observed due to the presence of tungsten oxide in the TiO_2 network. According to Leghari *et al*., [3], incorporating WO_3 into the TiO_2 network hindered titanium crystallization, decreasing peak intensity and, consequently, in the crystallinity of anatase/rutile nanocrystals. Tungsten ions are integrated into the TiO_2 network, replacing titanium ions and forming W-O-Ti bonds located in interstitial sites [9].

The diffraction patterns of $TiO_2/Na_2WO_4.2H_2O$ samples sintered at 200°C are shown in Figure 5. Sodium tungsten has a tetrahedral structure, whereas tungsten is surrounded by 4 toxicity atoms, forming WO_4 clusters with a tetrahedral crystalline.

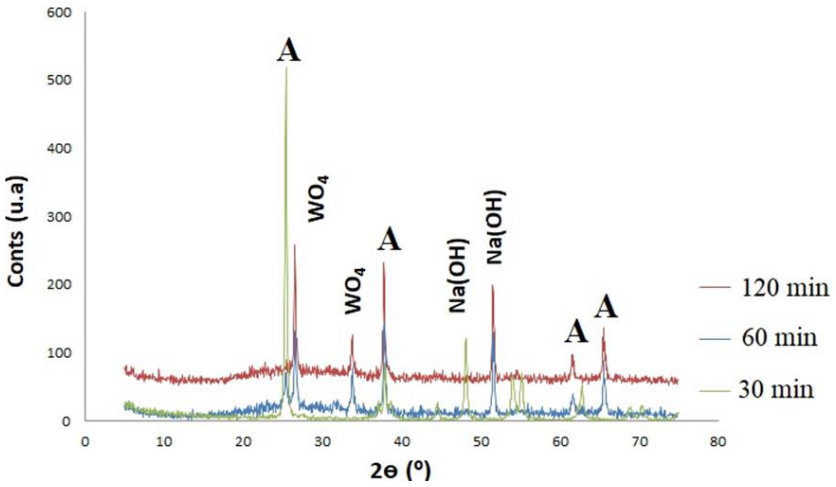

Figure 5 Caption 3. Diffractogram of $TiO_2/Na_2WO_4.2H_2O$ sample sintered at 200°C.

3.2 Scanning Electron Microscopy (SEM)

Figure 6 shows scanning electron microscopy (SEM) images of samples obtained by microwave-assisted hydrothermal synthesis. When analyzing these images, it is possible to observe that the

TiO_2 sample (Figure 2a) consists of irregularly shaped aggregates and interconnected pores. Analyzing the TiO_2/WO_3 and $TiO_2/Na_2WO_4.2H_2O$ samples, Figure 6b and Figure 6c, respectively, it is possible to observe that the samples have remarkable similarity in morphology, presenting clusters of large portions. These agglomerates are constituted by a mixture of the primary particles of TiO_2 and WO_3 [3, 10, 11]. The formation of particle aggregates observed in the samples, regardless of the synthesis temperature, occurs due to the state of supersaturation of the tungsten oxide crystals, generating a mixed formation between TiO_2 and WO_3 particles. Costa also observed this [8]. He verified the formation of agglomerates in the form of heterogeneous irregular plates formed by fine particles. Figure 6 illustrates the SEM images of pure TiO_2 and different composite samples. The SEM image of pure TiO_2 shown in Figure indicates that pure TiO_2 consists of irregular shapes and aggregates. The addition of dopants (H_2WO_4 and $Na_2WO_4.2H_2O$) has a significant effect on the morphology of the samples and increases loose aggregates. Which consequently significantly increases the interparticle voids and the level of aggregation of TiO_2 particles.

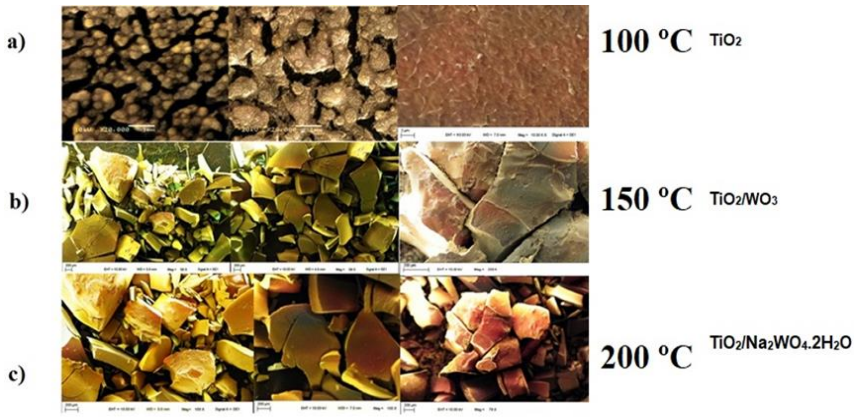

Figure 6 Caption 3. SEM images of samples of (a) TiO_2, (b) TiO_2/WO_3 and (c) $TiO_2/Na_2WO_4.2H_2O$, obtained at 100°C, 150°C and 200°C for 30, 60 and 120 minutes, respectively.

Figure 7 confirms the results presented in Table 1, where the pore size distribution range determined by the International Union of Pure and Applied Chemistry (IUPAC) is located in the mesoporous region between 2~50 nm. And that the isotherms are type IV with H3 hysteresis curves. [1].

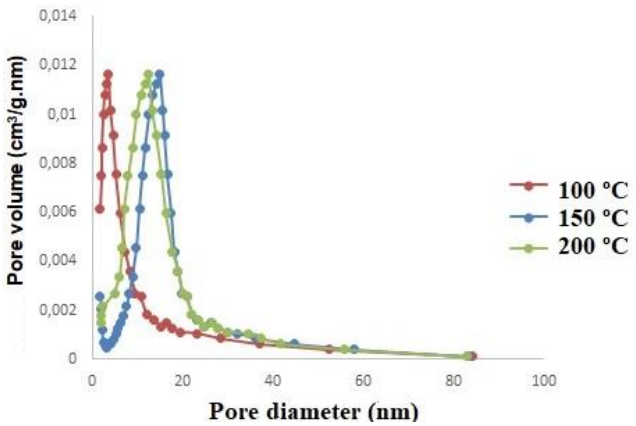

Figure 7 Caption 3. Pore diameter distribution of the samples obtained.

Table 1 Caption 3. Surface area, pore volume, and pore diameter values of the samples.

Samples	Surface area (m^2/g)	Pore volume (cm^3/g)	Poro diameter (nm)
TiO_2 P25 100°C	33.6	0.15	14.8
TiO_2 P25 150°C	31.0	0.14	15.8
TiO_2 P25 200°C	27.5	0.11	17.7
TiO_2 100°C	50.0	0.26	15.5
TiO_2 150°C	33.8	0.24	17.4
TiO_2 200°C	30.9	0.21	18.2
WO_3 100°C	249.8	0.54	20.2
WO_3 150°C	231.8	0.47	25.8
WO_3 200°C	187.5	0.34	27.2
TiO_2/WO_3 100°C	232.8	0.62	30.6
TiO_2/WO_3 150°C	126.4	0.58	33.4
TiO_2/WO_3 200°C	108.8	0.57	37.0
$TiO_2/Na_2WO_4.2H_2O$ 100°C	329.8	0.91	40.4
$TiO_2/Na_2WO_4.2H_2O$ 150°C	293.8	0.88	41.8
$TiO_2/Na_2WO_4.2H_2O$ 200°C	247.4	0.76	48.6

In general, the increase in the calcination temperature in the samples caused a decrease in the total pore volumes, an increase in the average pore diameter and a decrease in the surface area due to the sintering of the micropores. The data in Table 1 confirm this, as the TiO_2 samples sintered at a temperature of 100°C initially presented a pore volume of 0.15 cm^3/g and with the increase in temperature, there was a reduction up to 0.11 cm^3/g. The average pore diameter increased from 14.8 to 17.7 nm and the surface area decreased from 33.6 to 27.5 m^2/g.

It is worth remembering that the surface area of the semiconductor is a parameter that influences the heterogeneous photocatalysis process. Therefore, a semiconductor with a larger surface area presents a better photocatalytic response. However, other parameters, such as the crystalline phase and the energy gap value, also affect the efficiency of photocatalysis and are essential for the process [1].

The gradual decrease in the surface area value in samples is due to the particle sintering principle, the driving force of which is the reduction in surface area. The heat treatment used after synthesis causes the rupture of the tubular structure, thus reducing the value of the specific area [1].

Figure 8 and Figure 9 show the photocatalytic activity of TiO_2 P25 samples hydrothermally treated at 100°C, 150°C, and 200°C in 30, 60, and 120 minutes. Samples hydrothermally treated at 150°C and 200°C for 120 minutes were the most effective in decolorizing the methyl orange dye. They achieved an effectiveness of approximately 80% due to protonation.

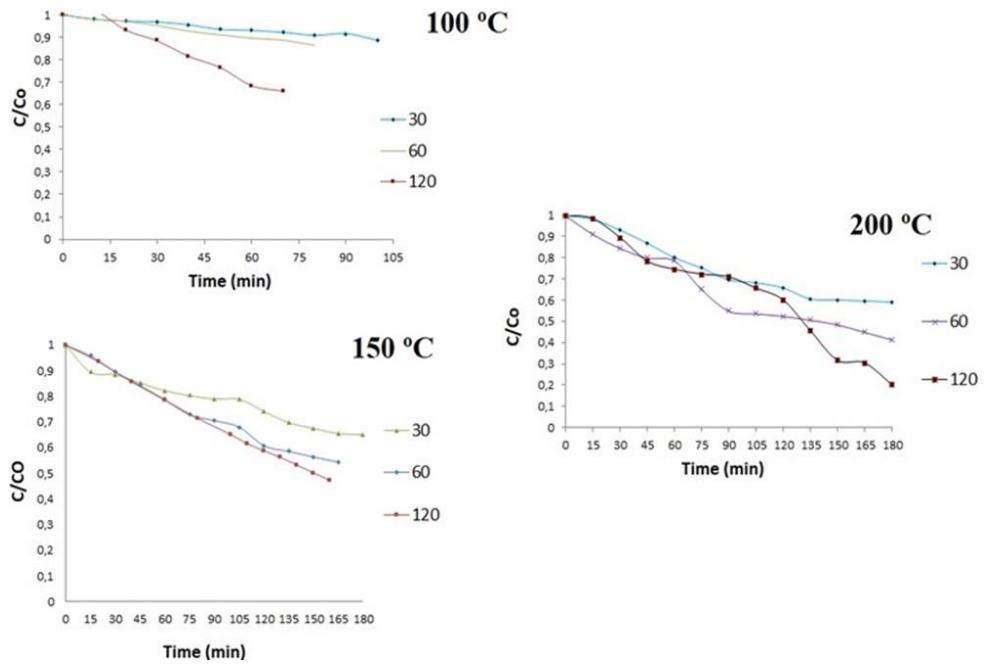

Figure 8 Caption 3. Photocatalytic performance of TiO_2 P25 samples in MO decolorization under UVA-vis light.

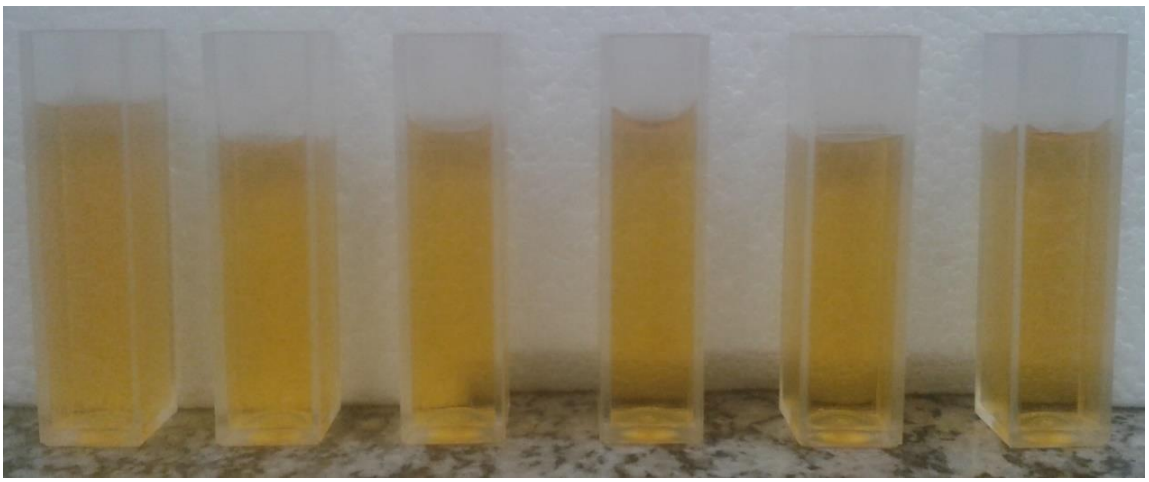

Figure 9 Caption 3. Polymethylmethacrylate cuvettes were used as semiconductors after the end of heterogeneous photocatalysis using TiO_2 P25 samples sintered at 200°C.

As a rule, protonation on the catalyst surface results from decreased pH in the system. It plays a fundamental role in photocatalytic activity, as it promotes the adsorption of organic compounds and/or some reactive species on surface surfaces. This TiO_2 growth process in the hydrothermal process occurs primarily in forming sodium titanate nanostructures in the alkaline equipment solution. The conversion into protonated titanate occurs through ion exchange of Na^+ and finally, the transformation of H^+ into TiO_2 occurs through thermal annealing [12, 13].

Because the methyl orange dye is an anionic dye, its layer on the examination surface is increased with the increase in positive charges on the oxide, which also contributed to obtaining the results for P25.

Figure 10 shows the photocatalytic activity of pure TiO_2 samples. The samples hydrothermally treated at 200°C were the most effective in decolorizing the methyl orange dye. They achieved an effectiveness of approximately 50% in decolorizing the MO dye.

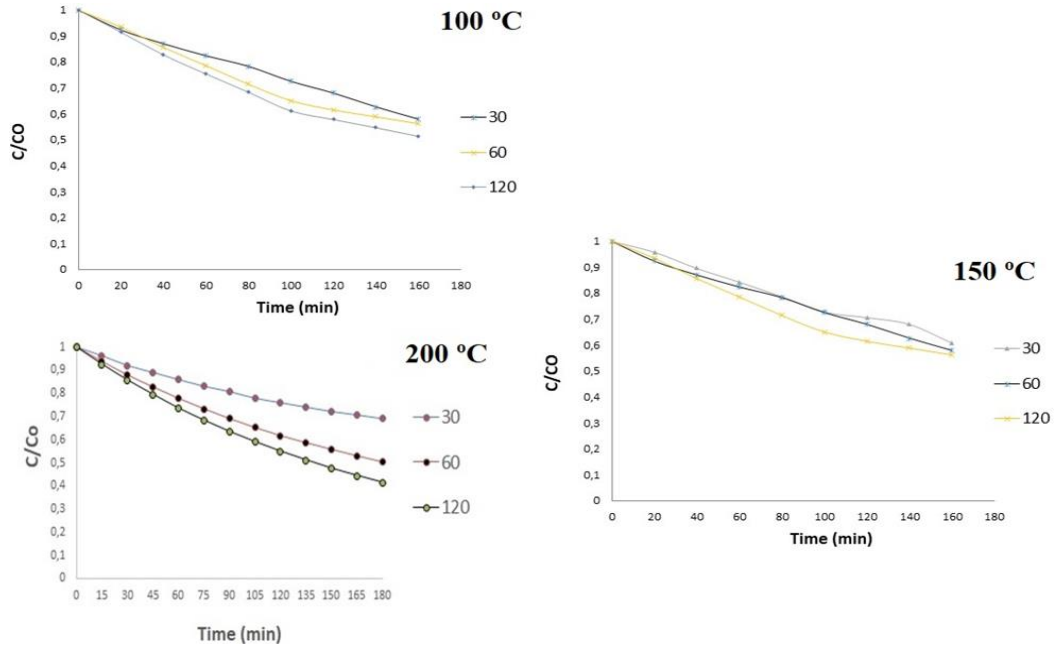

Figure 10 Caption 3. The photocatalytic performance of TiO_2 samples in MO decolorization under UVA-vis light.

As can be seen, the photodegradation capacity of samples increases with increasing analysis time, i.e., samples analyzed at 200°C for 120 minutes. When MO decolorization is increased, more dye molecules are adsorbed on the catalyst surface, occupying its active sites and reducing the generation of hydroxyl radicals on the photocatalyst surface. Furthermore, considering the Beer-Lambert law (Equation 2), there is a linear relationship between absorption (A) concentration (c) and molar absorption coefficient (ε) of a solution. When the concentration increases, the MO dye molecules absorb more radiation, and more molecules will be adsorbed on the catalyst's surface. Favoring the reaction between the dye molecules and the photogenerated holes or hydroxyl radicals [12, 13].

$$A = \varepsilon \times c \times l \quad (2)$$

Where:

A = absorption

C = concentration

Ɛ = molar absorption coefficient

l = the path length [12].

Visibly, the presence of tungsten precursors (H_2WO_4 and $Na_2WO_4.2H_2O$) in Figure 11 and Figure 12 were able to decolorize the MO dye under UVA-vis light, demonstrating significantly more excellent photocatalytic performance than pure TiO_2. According to the EDS, WO_3 obtained a band gap value of 2.8 eV, a band gap value lower than that obtained for pure TiO_2 of 3 eV. The lower band gap value of WO_3 allows the absorption of UVA light to be transferred to the visible light range,

improving photocatalytic activity. X-ray diffraction (XRD) showed that the intensity of the peaks from the TiO_2/WO_3 sample decreased compared to the peaks from the TiO_2 samples, indicating that the electron-hole pair's recombination occurred more slowly.

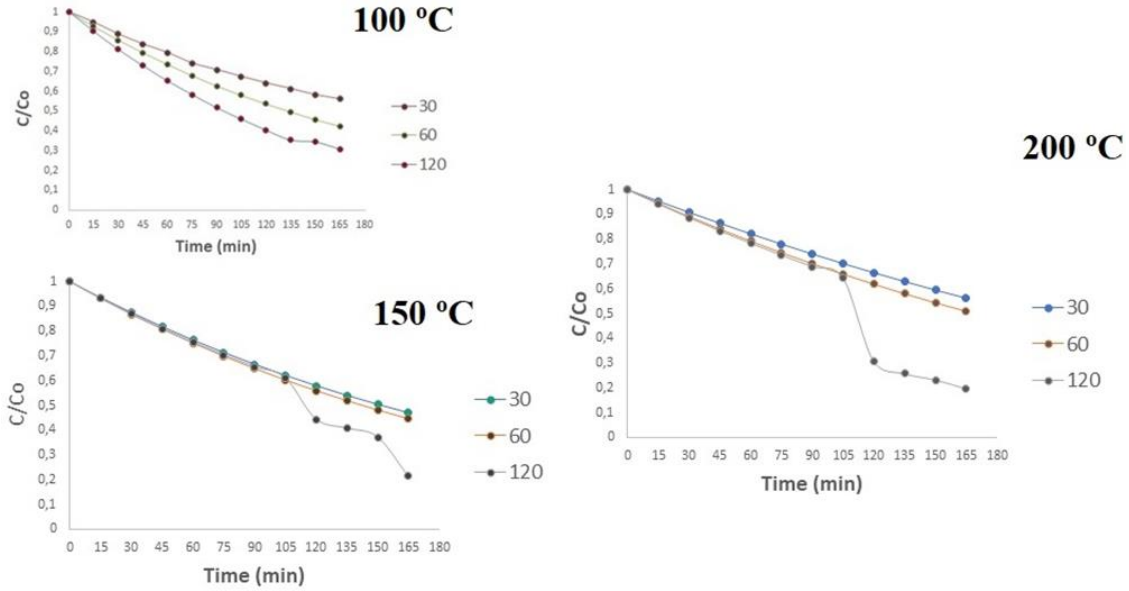

Figure 11 Caption 3. Photocatalytic performance of TiO_2/WO_3 samples in MO decolorization under UVA-vis light.

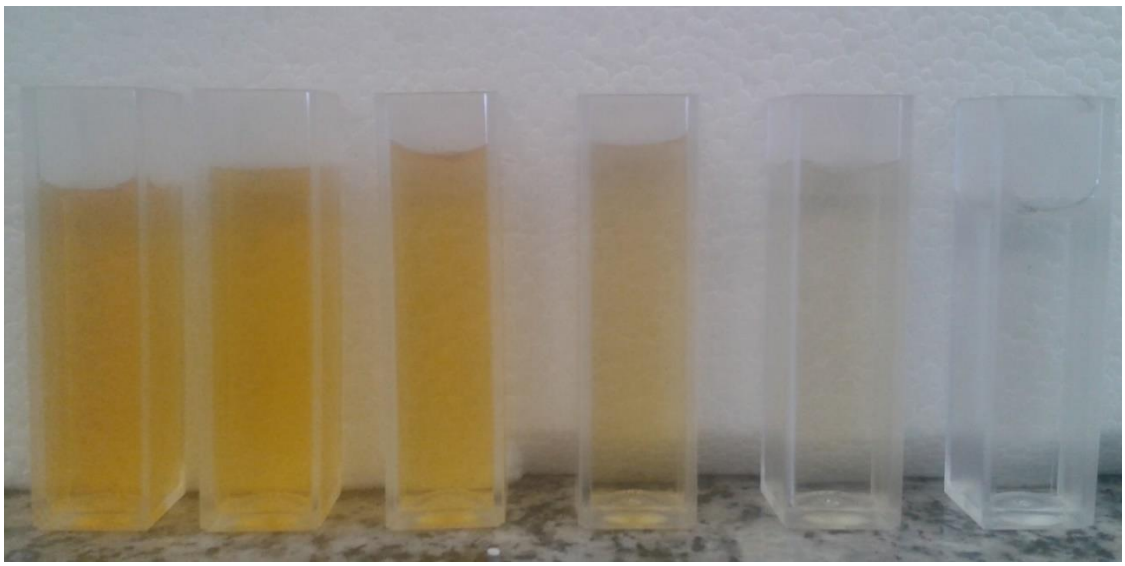

Figure 12 Caption 3. Polymethylmethacrylate cuvettes were used as semiconductors after the end of heterogeneous photocatalysis using TiO_2/WO_3 samples sintered at 200°C.

Photocatalytic performance of $TiO_2/Na_2WO_4.2H_2O$ samples in MO decolorization under UVA-vis light are shown in Figure 13 and Figure 14, respectively. According to The literature, the pure TiO_2 sample's chemical bonds are covalent. In other words, the chemical bond between the oxygen and titanium atoms on the surface is organized due to the covalent nature of the bond. Where the charges are ordered in the (110) direction, and the electronic distribution is shared between the

atoms, even between oxygens. This allows the organization of molecules adsorbed on the (001) surface of TiO_2 to form an epitaxial structure of surface charges. The binding energies of TiO_2 are located between approximately 460-465 eV. The presence of tungsten precursors caused a slight positive change in the TiO_2 network, such as forming the W-O-Ti bond [13, 14].

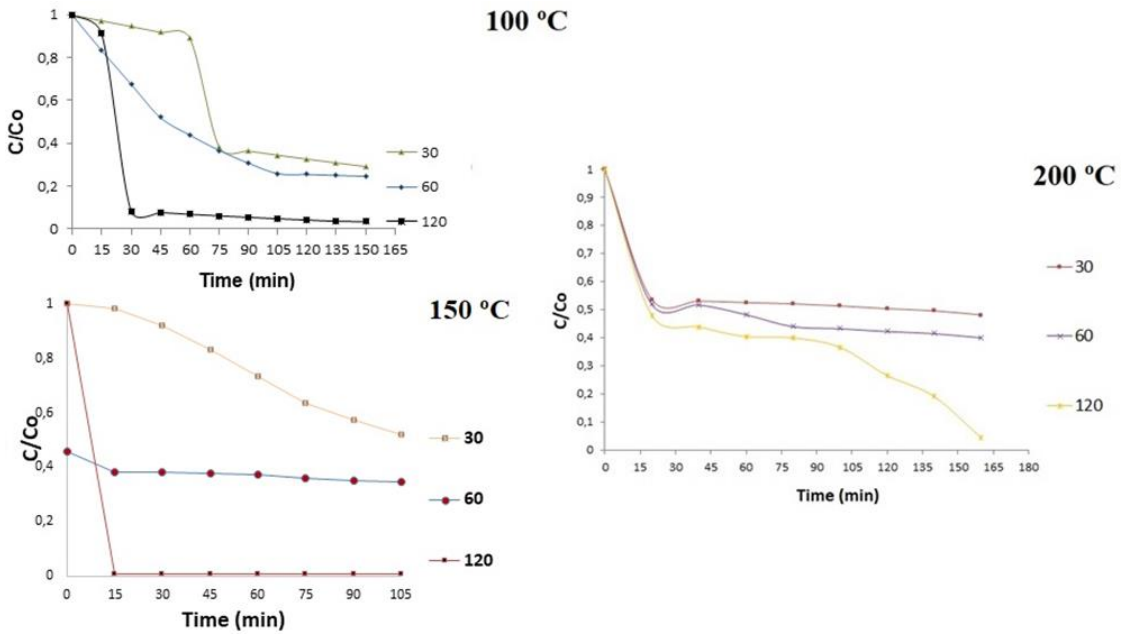

Figure 13 Caption 3. Photocatalytic performance of $TiO_2/Na_2WO_4.2H_2O$ samples in MO decolorization under UVA-vis light.

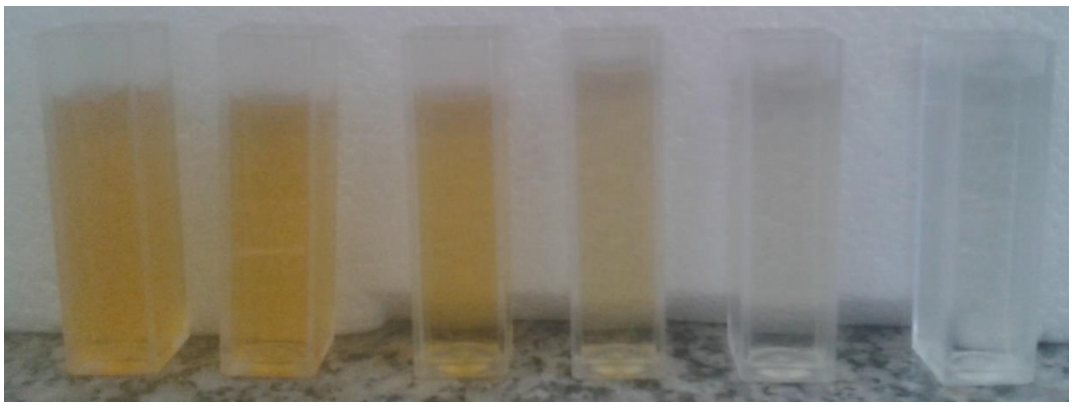

Figure 14 Caption 3. Polymethylmethacrylate cuvettes after the end of heterogeneous photocatalysis using $TiO_2/Na_2WO_4.2H_2O$ samples sintered at 150°C as semiconductors.

Figure 15 shows the degradation of orange when using WO_3 samples as photocatalysts. After 180 min of exposure to ultraviolet irradiation, all samples discolored approximately 100% of the methyl orange solution. In particular, all samples heat treated for 120 minutes could bleach 100% of this solution. Figure 16 samples synthesized for less time, 30 and 60 minutes, respectively, showed lower bleaching performance when compared to samples synthesized for 120 minutes.

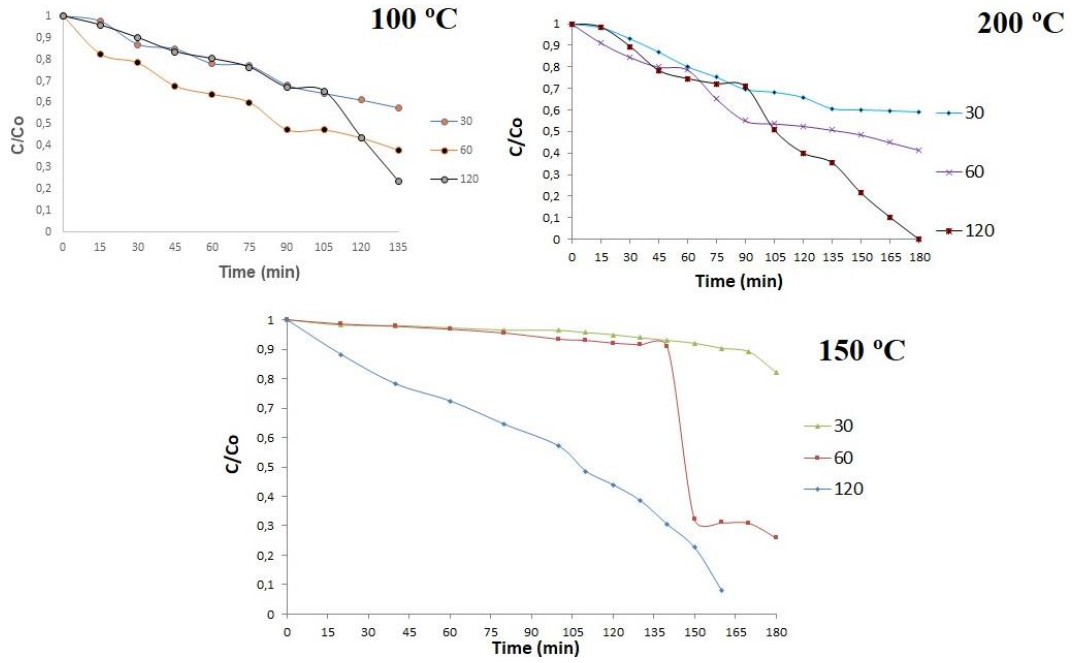

Figure 15 Caption 3. Photocatalytic performance of WO_3 samples in MO decolorization under UVA-vis light.

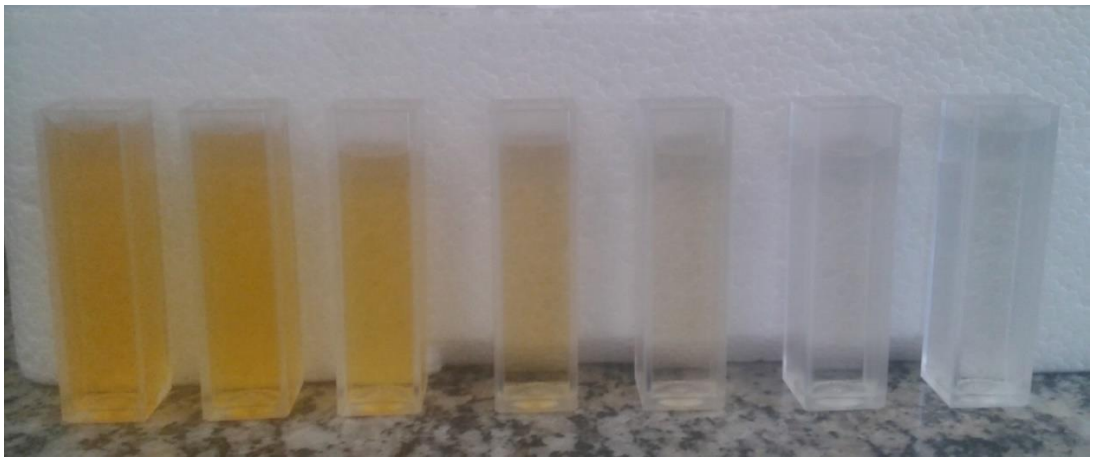

Figure 16 Caption 3. Polymethylmethacrylate cuvettes were used as semiconductors after the end of heterogeneous photocatalysis using WO_3 samples sintered at 150°C.

These results indicate that the temperature and radiation exposure time at which the powders are annealed play a fundamental role in the photocatalytic properties of WO_3 samples. The surface area of the photocatalyst is also a determining parameter in photocatalytic activity. As observed in Table 1, all WO_3 samples presented a high surface area, which generates a high concentration of defects in the crystalline structure of the oxide. WO_3 photocatalysts, under excitation with visible light, create electrons and holes, where electrons react with oxygen to produce hydroxyl radicals [4].

3.3 Diffuse Reflectance

The band gap values of all samples are presented in Table 2. These values are very relevant, as the distinction between semiconductor oxides or insulators is made based on the occupation of energy bands. Table 2 shows a reduction in the band gap of the fibers as the temperature increases calcination. This temperature increase favors the material's optical properties and the surface effects on the distribution of electronic levels. Also, it allows these samples to decrease the recombination of the electron/hole pair charges, allowing the transfer of charges between the two oxides (TiO_2 and WO_3), increasing the light absorption capacity [15].

Table 2 Caption 3. Band gap values of samples obtained by Microwave-assisted Hydrothermal Synthesis.

Samples	Band gap energy (ev)
TiO_2 P25 100°C	3.44
TiO_2 P25 150°C	3.10
TiO_2 P25 200°C	3.05
TiO_2 100°C	2.93
TiO_2 150°C	2.85
TiO_2 200°C	2.82
WO_3 100°C	2.58
WO_3 150°C	2.52
WO_3 200°C	2.49
TiO_2/WO_3 100°C	2.84
TiO_2/WO_3 150°C	2.78
TiO_2/WO_3 200°C	2.67
$TiO_2/Na_2WO_4.2H_2O$ 100°C	2.32
$TiO_2/Na_2WO_4.2H_2O$ 150°C	2.28
$TiO_2/Na_2WO_4.2H_2O$ 200°C	2.14

In intrinsic semiconductors, as in the case of the samples synthesized in this work, the band gap energy (Eg) is characterized by a filled valence band and a conduction band. It is through the thermal or optical excitation of electrons that an energy gap is formed in the valence band, and electrons are promoted to the valence band. As the temperature increases, the band gap of the samples decreases, and disorder in their electronic structure is generated, favoring their optical properties [7].

3.4 Colorimetry

The equipment records various information for each analysis, but the most useful for defining the color index are those from the CIE-Lab system. In this system, color is recorded as coordinates in a 3-axis system, with the a* (red and green) and b* (yellow and blue) axes varying between positive and negative values and L* (luminescence) varying between 0 and 100%. Negative values of a* represent the influence of green, and positive values of a* represent the influence of red. Negative values of b* represent the influence of blue and positive values of b* represent the

influence of yellow. On the L* axis, 0% represents black (total absence of reflected light) and 100% represents white (total reflection).

The results of the colorimetric tests performed on the TiO_2 P25 (standard), TiO_2, TiO_2/WO_3 and $TiO_2/Na_2WO_4.2H_2O$ samples are presented in Table 3. The records for each sample were obtained based on the CIE-L system *a* b and the measurement range covered the entire visible spectrum (400 to 700 nm). Table 1 also shows the luminescence values (% L), that is, the amount of light that is perceived in a given color. If the luminescence (% L) is close to 0%, it represents the total absence of reflected light (black) and if it is close to 100%, it represents the total reflection of light (white) [15]. And the ΔL* values inform the differences between lighter or darker shades. Positive (+) ΔL* values indicate lighter color and negative (-) ΔL* values indicate darker color. During the colorimetric tests, the P25 standard and the TiO_2 samples had maximum absorbance in the dark blue region, influenced by the positive values of a* (red color) and negative values of b* (blue color). The dark tone of the samples was determined based on negative ΔL* values. The TiO_2/WO_3 samples had maximum absorbance in the light blue color region, influenced by negative values of a* (green color) and negative values of b* (blue color). The light hue of the samples was determined based on positive ΔL* values. The maximum absorbance in the blue region reached by the TiO_2 and TiO_2/WO_3 occurs in the area of complementary color to blue; in this case, the complementary color is yellow. Finally, the $TiO_2/Na_2WO_4.2H_2O$ samples showed maximum light transmittance in the yellow-orange region, influenced by the positive values of a* (red color) and b* (yellow color). Therefore, the color absorbed by the $TiO_2/Na_2WO_4.2H_2O$ samples was blue-purple, which is complementary to orange-yellow [15]. All WO_3 samples showed an intense yellow color. They were influenced by the negative values of a* and the positive values of b*. Furthermore, it is worth remembering that the color of the precursor solution for synthesizing samples from this reagent (H_2WO_4) is yellow. The P25 standard and the TiO_2, TiO_2/WO_3, and $TiO_2/Na_2WO_4.2H_2O$ presented a good amount of perceived light, in agreement with the luminescence values (% L) shown in Table 3. In the synthesized samples, light radiation was absorbed by transitions that occur from the valence band to the conduction band, with a part being re-emitted at specific wavelengths. This was only possible because the samples synthesized semiconductors with band spacing between 2.24 eV and 3.24 eV. In this case, absorption and transmission occurred, and the color resulting from the interaction between the transmitted frequencies and those re-emitted after absorption. In the case of $TiO_2/Na_2WO_4.2H_2O$ samples, the color manifestation occurred through absorption at specific wavelengths. The color observed is the result of the combination of transmitted wavelengths.

Table 3 Caption 3. The colorimetry data obtained for the samples was obtained by hydrothermal means.

Samples	a*	b*	L%	ΔL Difference of tonality	Region of complementary color	Color (Region of maximum absorbance)
P25 30	+2.64	-3.44	57.78	-75.02	Yellow	Dark-blue
P25 60	+4.96	-2.94	61.96	-75.04	Yellow	Dark-blue
P25 120	+2.42	-5.76	57.01	-91.81	Yellow	Dark-blue
TiO_2 30	+1.46	-3.86	61.04	-83.62	Yellow	Dark-blue
TiO_2 60	+3.92	-1.88	51.07	-46.94	Yellow	Dark-blue

TiO_2 120	+1.84	-2.82	54.38	-87.82	Yellow	Dark-blue
WO_3 100°C	-5.34	+2.97	68.2	+68.42	Blue	Yellow
WO_3 150°C	-4.82	+7.86	86.4	+76.38	Blue	Yellow
WO_3 200°C	-1.39	+4.72	92.76	+94.57	Blue	Yellow
TiO_2/WO_3 30	-1.64	-2.42	87.67	+79.44	Yellow	Light-blue
TiO_2/WO_3 60	-1.40	-4.21	80.26	+70.31	Yellow	Light-blue
TiO_2/WO_3 120	-1.36	-2.53	82.81	+98.76	Yellow	Light-blue
$TiO_2/Na_2WO_4.2H_2O$ 30	+1.34	+5.75	51.618	-64.84	Blue-purple	Orange-yellow
$TiO_2/Na_2WO_4.2H_2O$ 60	+1.04	+3.62	58.67	-67.08	Blue-purple	Orange-yellow
$TiO_2/Na_2WO_4.2H_2O$ 120	+1.74	+7.04	64.84	-62.24	Blue-purple	Orange-yellow

4. Discussion

In this work, the photodegradation of methyl orange dye was successfully used to evaluate the photocatalytic activity of pure TiO_2-P25, used as standard and composite catalysts. It was observed that the catalysts showed excellent activity in the degradation of methyl orange dye (MO) under UVA-vis illumination. When irradiated with UVA-vis light, the semiconductors synthesized in this work were photocatalytically activated with radiation greater than or equal to the band gap energy, thus enabling the migration of electrons from the valence band to the conduction band, generating positive holes in the valence band. Which degraded the dye and reflected/absorbed light, changing the material's color [15, 16].

In colorimetry, electrons from the valence band, occupied only by the 2p orbitals of O, are promoted to the conduction band, occupied by the 5d orbitals of W, forming electron/hole pairs (e^-/h^+). The presence of tungsten precursors allowed the W^{6+} sites to capture electrons that are promoted to the conduction band, causing the reduction of ions. The holes dissociated H_2O molecules or proton-donating organic molecules, which are adsorbed on the surface of the particles. The reflection/absorption of light changes the color of the material, generating positively charged O_2 holes that capture the photoexcited electrons [14, 15].

Our results are confirmed by the authors below, who obtained results similar to ours by synthesizing TiO_2 and TiO_2/WO_3 catalysts.

In 2018, Soares *et al*. [1, 15] described the photocatalytic properties of TiO_2 and TiO_2/WO_3 films applied as semiconductors in heterogeneous photocatalysis. The results indicate that the fiber-based films showed good photoactivity and can be used as photocatalysts since the doping of TiO_2 films with tungstic acid (H_2WO_4) improved the photocatalytic efficiency of the materials by significantly reducing the band gap of TiO_2 [1, 15].

In 2023, Feng *et al*. [12] obtained nanostructured TiO_2 films by hydrothermal synthesis, transformed from titanates, at different treatment times. The results demonstrated that TiO_2 nanostructures transformed from titanates could be used in a photoelectrochemical system with PEC characteristics and adjusted and modified for better water-splitting performance [12].

Also, in 2023, Sharifiyan *et al*. [13], using the PEO/hydrothermal method, created a hierarchical TiO_2/WO_3 semiconductor with a hybrid coating for photocatalytic application. The results showed that the transient photocurrent measurements were successfully adjusted, and consequently, the catalysts are adequate for the most varied applications, such as photocatalysis [13].

Anson *et al*., 2024 [14] developed and modeled TiO_2 photoanodes for PEC water splitting: decoupling the influence of intrinsic material properties and film thickness. They found that the capacitance coefficients and transient activation kinetics depend on the thickness of the TiO_2 layer, indicating that the steady-state regimes are mediated by light accessibility. This behavior observed in the TiO_2 photoelectrode aims to facilitate further improvements in the efficiency of materials and electrodes for green hydrogen production [14].

In 2018, Soares *et al*. [15] described the correlation between titanium and tungsten oxide films when exposed to UV-A radiation due to similar phenomena. The results showed that the movie presented good photochromic and photocatalytic properties due to the synchronization between the chemical and physical properties of TiO_2 and tungsten [15].

Pan *et al*., in 2015 [9], hydrothermally obtained WO_3 films deposited on TiO_2 substrates and analyzed their photochromic properties at different concentrations. The results showed that with increasing precursor concentration, the absorptions observed at 365 nm of the films increased to a precursor concentration of 0.016 M, then decreased with higher concentration. The movie with a precursor concentration of 0.016 M on the TiO_2 substrate showed the best photochromic properties [9].

In a study carried out in 2023 by Ejeromedogene *et al*., [17] tungsten oxide was doped with TiO_2, using choline chloride/urea deep eutectic solvents (DESs), by hydrothermal/solvothermal synthesis in the presence of distilled water (H_2O), ethanol (EtOH), and isopropyl alcohol. The results obtained are promising and may open new insights for the development of photochromic materials, optical display devices and materials for glass/window coatings [17].

In the work carried out by Lázaro *et al*., [18] an investigation was carried out on volume and surface models (maximum 20 layers) of the TiO_2 material in the (001) direction. Their results were used to calculate energy surface, electronic levels, surface atomic displacement and change maps. The atoms in the first and second layers of the plate model showed very well-organized electronic densities in the form of chains or wires [18].

In 2023 Khalid et al. [19] synthesized WO_3 NPs using a facile hydrothermal method aided by polyvinylpyrrolidone (PVP). The authors found that the nanocomposites were highly influential in environmental remediation of antibiotics [19].

5. Conclusions

All synthesized samples showed photocatalytic activity. in the degradation of methyl orange dye. It was observed that catalysts containing tungsten precursors showed the best results in the degradation of methyl orange dye (MO) under UVA-vis illumination. The TiO_2/WO_3 $TiO_2/Na_2WO_4.2H_2O$ composite photocatalysts showed even higher photocatalytic activity than pure TiO_2 and agree with the mentioned results. Because they were efficient in degradation and saved energy. This makes this a promising method of obtaining materials for the most diverse applications, mainly in removing organic pollutants.

Acknowledgments

This work was carried out with the support of the National Council for Scientific and Technological Development (CNPq), a Brazilian government entity focused on training human resources. The authors would also like to thank the financial support of Brazilian agencies:

Coordination for the Improvement of Higher Education Personnel (CAPES), Research Support Foundation of the State of Rio Grande do Sul (FAPERGS) and Financier of Studies and Projects (FINEP).

Author Contributions

The authors of the manuscript contributed to the writing of the manuscript as follows. Luana Góes Soares writing, methodology, analysis of results, conclusions and general review. Sandra Kunst general review. Cláudia Trindade general review. Annelise Alves methodology and general review.

Competing Interests

The authors have declared that no competing interests exist.

References

1. Soares L, Alves A. Photocatalytic properties of TiO_2 and TiO_2/WO_3 films applied as semiconductors in heterogeneous photocatalysis. Mater Lett. 2018; 211: 339-342.
2. Thakur N, Thakur N, Kumar K. Nanoesferas de TiO_2 estabilizadas fitoquimicamente e com PVP para maior eficiência fotocatalítica e antioxidante. Mater Hoje Comun. 2023; 35: 105587.
3. Leghari SA, Sajjad S, Chen F, Zhang J. WO_3/TiO_2 composite with morphology change via hydrothermal template-free route as an efficient visible light photocatalyst. Chem Eng J. 2011; 166: 906-915.
4. Yuju S, Xiujuan T, Dongsheng S, Zhiruo Z, Meizhen W. A review of tungsten trioxide (WO_3)-based materials for antibiotics removal via photocatalysis. Ecotoxicol Environ Saf. 2023; 259: 114988.
5. Sun S, Ma H, Zhang Y, Yong M. Preparation and characterization of tungstated $Ce_xZr_{1-x}O_2@TiO_2$ solid superacid with promoting mass transfer. Microporous Mesoporous Mater. 2019; 284: 90-97.
6. Schabbach LM, dos Santos BC, De Bortoli LS, Fredel MC, Henriques B. Application of Kubelka-Munk model on the optical characterization of translucent dental zirconia. Mater Chem Phys. 2021; 258: 123994.
7. Chang JA, Vithal M, Baek IC, Seok SI. Morphological and phase evolution of TiO_2 nanocrystals prepared from peroxotitanate complex aqueous solution: Influence of acetic acid. J Solid State Chem. 2009; 182: 749-756.
8. Costa AC, Vilar MA, Lira HL, Kiminami RH, Gama L. Síntese e caracterização de nanopartículas de TiO_2. Cerâmica. 2006; 52: 255-259.
9. Pan L, Shen Y, Li Z. Hydrothermal synthesis of WO_3 films on the TiO_2 substrates and their photochromic properties. Mater Sci Semicond Process. 2015; 40: 479-483.
10. Liu M, Luo L, Dong F. Characteristics and mechanism of photocatalytic uranium removal enhanced by hole-scavenging citric acid chelation in a TiO_2 suspension system. J Radioanal Nucl Chem. 2019; 319: 147-158.
11. Ahmadi M, Younesi R, Guinel MJ. Synthesis of tungsten oxide nanoparticles using a hydrothermal method at ambient pressure. J Mater Res. 2014; 29: 1424-1430.

12. Feng T, Yam FK. The influence of hydrothermal treatment on TiO_2 nanostructure films transformed from titanates and their photoelectrochemical water splitting properties. Surf Interf. 2023; 38: 102767.
13. Sharifiyan MS, Fattah-alhosseini A, Karbasi M. Photocatalytic evaluation of hierarchical TiO_2/WO_3 hybrid coating created by PEO/hydrothermal method. Appl Surf Sci Adv. 2023; 18: 100541.
14. Ansón-Casaos A, Ciria JC, Martínez-Barón C, Villacampa B, Benito AM, Maser WK. Modelling TiO_2 photoanodes for PEC water splitting: Decoupling the influence of intrinsic material properties and film thickness. Int J Hydrog Energy. 2024; 52: 1146-1158.
15. Soares L, Alves A. Analysis of colorimetry using the CIE-L*a*b* system and the photocatalytic activity of photochromic films. Mater Res Bull. 2018; 105: 318-321.
16. Soares LG, Alves AK. Obtaining TiO_2 nanostructures by electrospinning and analysis of absorbance in the UVA spectrum for photocatalytic application. Catalysis Res. 2023; 3: 016.
17. Ejeromedoghene O, Kpomah B, Daramola CB, Abesa S, Adewuyi S, Fu G. Deep eutectic co-solvent mediated surface-enhanced photochromic property of tungsten oxide doped titanium oxide (WO_3-TiO_2) heterostructures. Sci Talks. 2023; 5: 100149.
18. Lazaro SD, Penteado RF, Tebcherani SM, Berger D, Varela JA, Kubaski ET. Energia de superfície para nanossuperfícies de TiO_2 na direção (001). Quim Nova. 2012; 35: 920-923.
19. Alzahrani KA, Ismail AA. Highly efficient $AgVO_3/WO_3$ photocatalyst nn heterojunction toward visible-light induced degradation antibiotic. J Ind Eng Chem. 2023; 124: 270-278.